

Free Energy of Scission for Sodium Laureth-1-Sulfate Wormlike Micelles

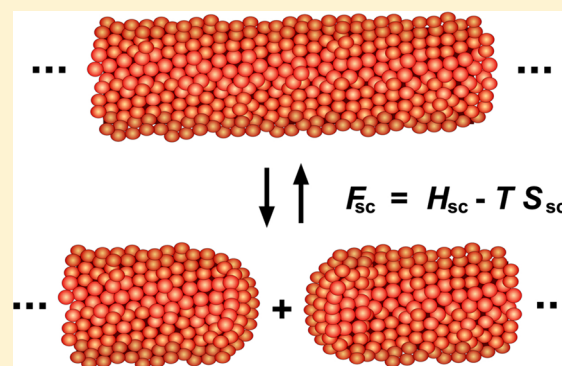
Karsten Vogtt,^{*,†} Hanqiu Jiang,[†] Gregory Beaucage,^{*,†} and Michael Weaver[‡]

[†]Biomedical, Chemical, and Environmental Engineering, University of Cincinnati, Cincinnati, Ohio 45221, United States

[‡]P&G Analytical Sciences, 8700 Mason-Montgomery Road, Mason, Ohio 45040, United States

Supporting Information

ABSTRACT: Wormlike micelles (WLMs) are nanoscale, self-assembled components of many products from shampoos to fracking fluids due to their viscoelasticity. Their rheological behavior is largely governed by the contour length of the micelles and the concomitant propensity of the micelles to overlap and entangle. The large contour lengths, on the order of micrometers, is the result of a delicate balance between the scission enthalpy of the wormlike micelles on the one hand and entropic factors such as the mixing entropy of dispersion, the ordering of water molecules and counterions, and the mobility of branch points on the other hand. The structure and contour length of wormlike micelles assembled from sodium laureth-1-sulfate was determined at various temperatures using small-angle neutron scattering. The results allow the calculation of the enthalpy and entropy as well as the free energy of scission and are employed to critically evaluate the common methods to determine micellar scission energy from mean-field theory. Interesting behavior is observed when comparing branched and unbranched WLMs that may reflect on mechanistic differences in chain scission.



INTRODUCTION

Wormlike micelles (WLMs) can be assembled from surfactant molecules in an aqueous environment. At surfactant concentrations just above the critical micelle concentration, usually spherical or ellipsoidal micelles are formed. Increasing surfactant concentration creates additional micelle aggregates up to the second critical micelle concentration.¹ Further addition of surfactant or salt beyond the second critical micelle concentration induces the growth of WLMs.² WLMs can be envisioned as self-avoiding chains formed by cylindrical segments. The presence of these extended structures has a large impact on the viscoelastic properties of the dispersion; e.g., the zero-shear viscosity drastically increases. The fully extended conformation of the WLM, as it is induced by the application of shear, for example, is entropically unfavorable. Hence a population of WLMs exerts resistance to external mechanical forces. This entropic elasticity is utilized in formulations for thickeners and drag reducers in products such as shampoos.^{3,4}

One major factor contributing to the macroscopically observable viscosity is the contour length L of the WLMs. Depending on the experimental conditions, the viscosity can exhibit different dependences on L . Under dilute conditions, in the absence of entanglements, the specific viscosity η_{sp} is expected to scale with $\sim L^{3/2}$.⁵ A much stronger dependence is expected above the entanglement concentration. The forces governing the overall length of the WLMs are therefore of crucial interest. Particularly interesting is the observation that

the zero-shear viscosity first increases and then decreases at very high salt concentrations, i.e., that the zero-shear viscosity exhibits a maximum value in surfactant or salt concentration.² It has been suggested that this finding is due to the onset of branching at high salt concentrations. It is proposed that viscosity decreases because the branch points are mobile and can contribute to stress relaxation.⁶

In the mean-field theory of Cates and Candau, the average contour length L is associated with the chain scission energy E_{sc} by following the scaling relationship

$$L \propto \phi^{1/2} \exp\left(\frac{E_{sc}}{2k_b T}\right) \quad (1)$$

where ϕ is the volume fraction, k_b is the Boltzmann constant, and T is the absolute temperature. The formula is valid for neutral or electrostatically highly screened systems. E_{sc} is the excess free energy required to create two new chain ends as compared to a rodlike geometry with a similar number of surfactant molecules.⁷ Works reporting values for E_{sc} for WLM systems are scarce.^{8–19} Most studies were carried out using the cationic surfactant cetyltrimethylammonium and yielded scission energies E_{sc} of between 50 and 120 kJ mol⁻¹. Usually E_{sc} is calculated indirectly using rheological methods employing

Received: March 25, 2016

Revised: January 25, 2017

Published: January 30, 2017

the activation energies for breakage and the terminal relaxation time.^{8,9} For an aqueous dispersion of cetyltrimethylammonium bromide in the presence of potassium bromide, a value of $E_{sc} \approx 60 \text{ kJ mol}^{-1}$ has been reported.⁸ For the same surfactant cation in the presence of sodium chloride and sodium salicylate, however, an E_{sc} of twice this value has been reported and has been rejected as unrealistically large.¹⁰ Siriwatwechakul et al. report values of between 70 and 80 kJ mol^{-1} for erucyl bis(hydroxyethyl) methylammonium chloride in the presence of potassium chloride as well as ethanol or hexane.¹⁸ Couillet et al. investigate the same surfactant in the presence of 2-propanol and discuss that large values of E_{sc} lead to unrealistically large contour lengths.¹⁷

As a possible solution to the problem of an excessively large E_{sc} , it has been suggested that the energy determined according to scaling [relation 1](#) might reflect only the enthalpic part of the scission free energy.^{16,17} Accordingly, the energy E_{sc} in [eq 1](#) is more precisely an enthalpy H_{sc} lacking the entropic contribution. The negative contribution to free energy due to a hypothetical entropic term could adjust the overall free energy to values that could predict reasonable contour lengths. In the context of the scaling relationship ([eq 1](#)), this proposition would add a temperature-independent constant to the expression. Under the assumption that this constant can be neglected, Couillet et al. find that low ionic strength and highly binding counterions lead to large H_{sc} ,^{11,14,15} whereas high ionic strengths and salt screening go along with low scission enthalpies, H_{sc} .^{9,17}

All of the cited literature works employ rheology to calculate E_{sc} or H_{sc} in a model-dependent manner. Because every method has its approximations and limits, it would be useful to obtain H_{sc} by employing complementary methods. Here, methods directly accessing the structure are especially suitable. Small-angle neutron scattering (SANS) directly accesses the spatial range from a few to hundreds of nanometers and is therefore an appropriate technique for this task. The hydrophobic core of WLMs is usually rich in hydrogen atoms, which yields a superior scattering length density contrast using neutrons as a probe and deuterium oxide as the solvent. We recently published a scattering function for small-angle scattering that is capable of characterizing the structure of wormlike chains.²⁰ Here, the WLMs are modeled as a chain consisting of cylindrical segments. Fitting the scattering intensity $I(q)$ with this function allows the determination of the length and radius of the cylindrical subunits as well as the total number of these subunits in a WLM. Moreover, the presence of branches can be detected and quantified. The determination of the length and number of the cylindrical subunits allows the calculation of the overall contour length L . If SANS measurements are performed at different temperatures T , then the contour length can be determined from the scattering intensity $I(q)$. Linear regression of the logarithm of L vs the reciprocal temperature yields H_{sc} according to scaling [relation 1](#).

In this work, the scattering intensity $I(q)$ has been determined for surfactant sodium laureth-1-sulfate (SLE1S) in the presence of 3.1 and 6.13 wt % NaCl in D_2O at different temperatures (15, 25, and 35 °C). As mentioned above, the zero-shear viscosity exhibits a maximum as a function of salt concentration. The salt concentrations in this study were selected to yield comparable values for the zero-shear viscosity left and right of this maximum as discussed in the [Results and Discussion](#) section. Using the recently published scattering function,²⁰ the contour lengths have been determined and the

scission enthalpy has been obtained according to scaling [relation 1](#) under the assumption that the entropic contribution is negligible. The accompanying results are compared to the results from the exact quantitative expression as outlined in the following [Theory](#) section.

THEORY

The scaling relationship of [eq 1](#) is derived from following the quantitative expression

$$\bar{N} = \phi^{1/2} \exp\left(\frac{E_{sc}}{2k_b T}\right) \quad (2)$$

where \bar{N} is the average number of surfactant molecules in a WLM. For a constant cross-sectional area $L \propto N$, scaling [relation 1](#) is obtained. [Relation 1](#) rather than [eq 2](#) is experimentally employed because the contour length is a convenient and more accessible parameter. However, from SANS, all of the important structural features of a WLM can be obtained and N can be quantitatively calculated.

Several scattering functions are available to fit SANS data from WLMs.^{20–22} The Pedersen–Schurtenberger (PS) model,²² for example, requires an independent computer simulation of a self-avoiding chain. This simulation is transformed to inverse space and further coupled with specifics of the wormlike chain. The PS model cannot accommodate chain branching. It relies on assumptions associated with the simulated chain. A recently published scattering model, described in [ref 20](#), is comparatively simple, does not require an independent chain simulation, and can account for branching. For these reasons, it was employed here. Within the SANS model of [ref 20](#), the WLMs are separated into structural levels, which additively contribute to the overall scattering. They are considered to consist of a chain with cylindrical segments. The first structural hierarchy is the cylindrical Kuhn subunit with index 1. Accordingly, L_1 and R_1 denote the length and radius of these cylinders. Index 2 refers to the structure of the chain formed by the interlinked cylinders. $L_2 = zL_1$ is thus the contour length of the overall chain, and z is the number of subunits. Because L_2 is calculated from measured values L_1 and z , it can display sizes larger than the size range accessed by the SANS measurement. That is, L_2 reflects the length of a hypothetically extended structure, and the observed structure is tortuous and has an overall size reflected in $R_{g,2}$, the radius of gyration for the WLM. L_2 is a weight average of the contour length.

With these parameters, N can be expressed via the mass of a cylindrical subunit m_{sub} and the mass of a single surfactant molecule m_{surf}

$$\bar{N} = \frac{m_{sub} z}{m_{surf}} \quad (3)$$

The mass of the surfactant molecule, m_{surf} , is known. In the present case, the average mass of the industrial-grade surfactant anions is 323 g mol^{-1} , which just slightly differs from that of the pure SLE1S anion of 309.4 g mol^{-1} ([Materials and Methods](#)). The mass of the cylindrical subunit can be calculated from its mass density ρ_m and its volume V_{sub} , the latter of which is obtained from the scattering measurement.

$$m_{sub} = \rho_m V_{sub} = \rho_m (\pi R_1^2 L_1) \quad (4)$$

The mass density of the SLE1S micelles is known to a good approximation ($\rho_m \approx 1.13 \text{ g mL}^{-1}$), and R_1 and L_1 are obtained

from the fit of the scattering intensity $I(q)$. Equation 2 can thus be rewritten as

$$\frac{\rho_m (\pi R_1^2)}{m_{\text{surf}}} L_2 = \phi^{1/2} \exp\left(\frac{E_{\text{sc}}}{2k_b T}\right) \quad (5)$$

Because eq 1 is a scaling relationship, it can only be used to study the dependence of L_2 for a series of temperatures, yielding the scission energy from an Arrhenius plot. However, as further discussed below, because eq 5 is an exact relationship, it can be rearranged to solve for E_{sc} for different temperatures. This allows the determination of both the enthalpy and entropy of scission because the temperature dependence of E_{sc} is now available. Generally, the parameters in eq 5 cannot be entirely determined using rheology, but they can be determined using SANS.

Whether the energies or enthalpies, respectively, yield consistent results can be checked by a comparison of the measured L_2 under different conditions with the ratio of theoretical L according to relation 1. If the theoretical results are not consistent, then E_{sc} can be extended for an entropic part as outlined in the Introduction,¹⁷

$$E_{\text{sc}} = H_{\text{sc}} - TS_{\text{sc}} \quad (6)$$

In this case, E_{sc} can be better identified as the free energy of scission, F_{sc} . Formula 5 can be rearranged to adapt the well-known identity of the Gibbs free energy.

$$2RT \ln\left(\frac{\rho_m (\pi R_1^2) L_2}{m_{\text{surf}} \phi^{1/2}}\right) = F_{\text{sc}} = H_{\text{sc}} - TS_{\text{sc}} \quad (7)$$

where R is the universal gas constant using the unit mol^{-1} . Equation 7 can be employed to cross check whether the addition of an entropic part, TS_{sc} , to E_{sc} can correct the inconsistencies found in previous works,¹⁷ particularly the prediction of unreasonably large L_2 values. All parameters on the left-hand side of eq 7 are known, and a plot of F_{sc} vs T yields H_{sc} and S_{sc} . H_{sc} in turn can be compared to the value from the previously used semilog plot according to scaling relation 1 used in all of the studies in the literature to date. If the values agree to within the error bars, then the assumption is supported that relations 1 and 2 are formally valid and merely require an entropic extension.

It should be noted that in eq 2, obtained from Cates theory,⁷ E_{sc} specifically *does not* include the mixing entropy associated with the WLM chain segments, which is dealt with in a separate term in the derivation. This leaves to conjecture the meaning of an entropic component of E_{sc} . It can be postulated that this change in entropy on WLM chain scission might be associated with a number of factors that are not included in the change in mixing entropy such as changes in the organization of water and counterions and/or loss of the mobility of WLM branch points along the chain. Furthermore, it might be expected that scission in branched WLMs could significantly and mechanistically differ from WLM scission in linear chains because there is a smaller energy penalty for the removal of a branch, which creates only one chain end, compared to scission of a linear chain, creating two energetically disfavored chain ends. Therefore, the stripping of branches could be a favored mechanism if branching is present and could result in a lower enthalpy change on scission and potentially a reduction in entropy on chain scission due to the loss of branch mobility along the WLM.

MATERIALS AND METHODS

Sodium laureth-1-sulfate (SLE1S) is 70% active STEOLCS170 purchased from Stepan (Northfield, IL) and used without further purification. The SLE1S surfactant with an average of one ethoxy (EO) group per molecule has a narrower chain length and EO distribution compared to other alkyl ethoxylate sulfate surfactants. D₂O 99.96% was obtained from Cambridge Isotope Laboratories, Inc. CryoTEM samples were prepared for analysis by placing $\sim 2 \mu\text{L}$ on a lacey carbon grid, blotting away the excess, and plunging the specimen rapidly into liquid ethane using a controlled environment vitrification system (CEVS). Once frozen, the samples were stored under liquid nitrogen until being loaded into a Gatan model 626 cryoholder. The specimens were then loaded into a Tecnai TEM and imaged at 120 kV in low-dose mode. The specimen was maintained below $-175 \text{ }^\circ\text{C}$ during transfer into the microscope and during analysis. Flow viscosity measurements were made using either a TA Instruments DHR3 rheometer with cup and bob geometry or an Anton Paar Lovis ME2000 rolling ball viscometer. For the DHR3, the temperature was controlled using a Peltier cup accessory, and a solvent trap was used to maintain the environmental integrity. The viscosity flow curves were collected using TRIOS software and steady-state sensing. The zero-shear viscosity was verified by measuring over several shear rate settings below 0.1 s^{-1} using steady-state averaging to verify the zero-shear viscosity plateau at shear rates below the onset of the shear-thinning region. The reported zero-shear viscosity was typically the average of several viscosity data points between 0.001 and 0.01 s^{-1} . SANS measurements were performed at the GP-SANS instrument at Oak Ridge National Laboratory in Oak Ridge, Tennessee, USA. Data reduction was performed using a plugin for the Igor Pro software provided by the instrument scientists. For the background subtraction, the scattering intensity $I(q)$ of the pure D₂O/NaCl solutions was employed.

The SANS model and the fitting procedure are described in detail in ref 20. Here, just principal points of the evaluation process will be explained. The scattering intensity $I(q)$ is considered to be a combination of individual scattering contributions $I_1(q)$ and $I_2(q)$ from the cylindrical subunits and the large-scale distribution of these objects, respectively. These intensity functions are combined using the unified approach.²⁰ The volume fraction times contrast squared $\phi(\Delta\rho)^2$ and the radius R_1 and length L_1 of the cylindrical subunits constituting the wormlike chain are gained from the fits. The radius is modeled as a polydisperse variable where R_1 denotes the median value and $\sigma_{R,1}$ denotes the corresponding dimensionless width parameter or the geometric standard deviation. All of these values allow the calculation of the scattering intensity at zero angle for the first structural level G_1 . As fitting parameters from the large-scale structure, the scattering intensity at zero angle G_2 , the radius of gyration $R_{g,2}$, and the fractal dimension $d_{f,2}$ are obtained. Here it is assumed that the overall wormlike chain performs a self-avoiding walk so that the minimum fractal dimension can be fixed to a value of $5/3$.²⁰ The knowledge of G_1 and G_2 allows the calculation of $z = G_2/G_1 + 1$, the weight-average number of subunits, and from this value, in turn, the branch content n_{br} . The contour length, $L_2 = zL_1$, can then be plotted according to eqs 1 and 7, yielding F_{sc} , H_{sc} , and S_{sc} .

Fits were performed using the Igor Pro software with a user-programmed algorithm in the case of the scattering function for $I(q)$ and a built-in function for the linear regression. For values derived from the fitting parameters such as the number of subunits z , error bars were calculated according to the propagation of error using the standard deviations obtained from the fits. The statistical error in the intensity was propagated through the fit routine.

RESULTS AND DISCUSSION

Background Rheology and TEM. It is of interest to use SANS to gain an understanding of the structural and thermodynamic basis for rheological observations, so samples have been chosen that are rheologically interesting. Rheological measurements of WLMs are largely restricted to surfactant

concentrations above 3% where significant chain entanglement occurs, whereas SANS, molecular modeling, and TEM measurements are generally limited to lower surfactant concentrations below 1% where individual chain structure can be observed. For this reason, it is challenging to identify samples that directly compare SANS and rheology.

The viscosity of WLMs changes as salt is added to an ionic surfactant solution. As salt is added, the end cap energy increases and the system reacts to by consolidating smaller micelles into fewer, longer ones. Longer micelles eventually entangle and greatly increase the viscosity. As the end-cap energy continues to increase with further addition of salt, micelle branching eventually becomes a significant mechanism for reducing the number of end-caps. Micelle branches are mobile and add extra degrees of freedom to escape entanglements, which leads to faster relaxation and reduces the viscosity.²³ This creates a peak in the viscosity curve as the salt is linearly increased. A curious consequence is that different surfactant–salt compositions can have the same viscosity because there is a maximum in the viscosity–salt concentration plot. However, the rheological frequency spectra of these isoviscosity points measured by an oscillatory sweep experiment clearly show that the micelle relaxation dynamics for these is different. This is evident in Figure 1, in which the NaCl

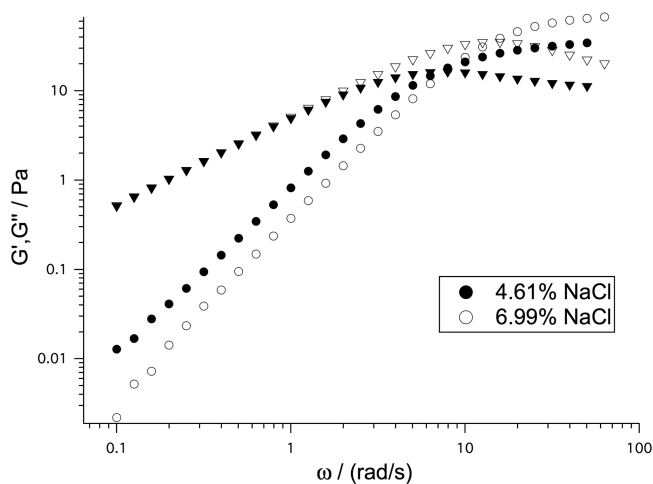


Figure 1. Complex frequency spectrum for two samples of equivalent zero-shear viscosity at 25 °C, with 5.0% SLE1S/D₂O at 4.61 (black) and 6.99% NaCl (white). The loss modulus G'' (inverted triangles) overlays in the terminal region, but the storage modulus G' and the rest of the spectrum do not. The larger NaCl concentration has a smaller relaxation time (higher frequency) consistent with a high level of branching.

concentration was used to adjust the viscosity to be the same (5.1 Pa·s) on either side (low salt concentration, linear; high salt concentration, branched) of the maximum in the salt–viscosity curve for 5.0% SLE1S/D₂O solution. The terminal G'' loss moduli (inverted triangles) of the two samples overlay as they should for same-viscosity samples, but the rest of the rheology spectrum does not. A Maxwell model fit to the data indicates that the relaxation time of the low salt (4.61% NaCl) is twice as long as that of the high salt (6.99% NaCl), 0.90 and 0.44 s, respectively. The shifts in frequency spectra to faster relaxation with increased NaCl is consistent with micelle branching (but other possibilities are not ruled out). A higher plateau modulus G_0 is observed for the sample with higher salt

content. This increase can be attributed to an additional contribution of branching points to the cross-link density. The smaller relaxation time for the larger-scale concentration curve is consistent with current theories for the effect on dynamics of branching in wormlike micelles.

Figure 2 shows how the viscosity of the solution changes with surfactant volume fraction ϕ_v for 3.10 and 6.13% NaCl/

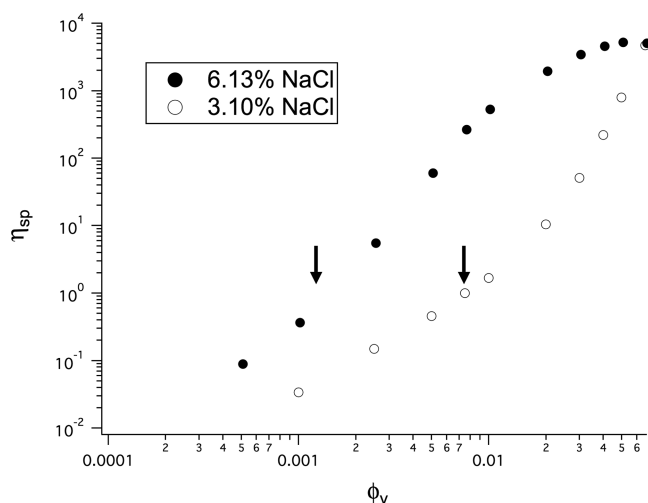


Figure 2. Relationship of specific viscosity η_{sp} with SLE1S volume fraction ϕ_v for 3.10% (predominantly linear) and 6.13% (predominantly branched) NaCl micelles. The arrows indicate the estimated volume fraction ϕ_v for the transition from the dilute to the semidilute regime.

D₂O. These salt concentrations were chosen on either side of the maximum in the viscosity–salt curve so that the same 6.67% SLE1S concentration would have similar η_{sp} but would have either predominantly linear micelle morphology for 3.10% NaCl/D₂O or predominantly branched micelles for 6.13% NaCl/D₂O. In Figure 2, the viscosity changes in moving from the semidilute to dilute regime, being diluted from 6.67% surfactant at fixed NaCl/D₂O concentration. The surfactant concentrations are plotted as the specific viscosity, η_{sp} ($= \eta_0 / \eta_{\text{solvent}} - 1$), against the density corrected volume fraction ϕ_v . η_{sp} corrects for the solvent viscosity contribution (NaCl/D₂O) and the density of added NaCl. Dilution from the same approximate viscosity ($\eta_{sp} \approx 5100$) and surfactant concentration (~ 220 mM, $\phi \approx 0.066$) shows a different evolution in viscosity as $\phi \rightarrow 0$ for the two salt concentrations. The 3.10% NaCl/D₂O linear micelles initially decrease with a power law slope of ~ 5.7 from $\phi \approx 0.067$ to approximately $\phi \approx 0.03$, which appears to be the entanglement concentration. The power law of 5.7 is in agreement with what is obtained for linear micelles in the so-called slow-breaking regime $\tau_{\text{break}} \gg \tau_{\text{rep}}$.²⁴ Oscillatory measurements at and below $\phi \approx 0.02$ show no evidence of entangled rheology. The slope in this semidilute regime is consistent with that found for the CTAB–NaNO₃ system reported by Helgeson and co-workers.²⁵ At and below $\phi \approx 0.01$, the viscosity falls off with a power law slope of ~ 1.7 . This is consistent with the model of Carale and Blankschtein,⁵ who predict that $\eta_{sp} \approx \phi(\xi L)^{3/2}$. Using eq 1, $L \approx \phi^{1/2}$, it is found that $\eta_{sp} \approx \phi^{1.75}$ in the dilute regime for WLMs that display the Cates' dependence of L on ϕ_v .

The dilution behavior of the branched 6.13% NaCl/D₂O sample is completely different. Starting from the highest concentration $\phi \approx 0.067$, the viscosity actually slightly increases

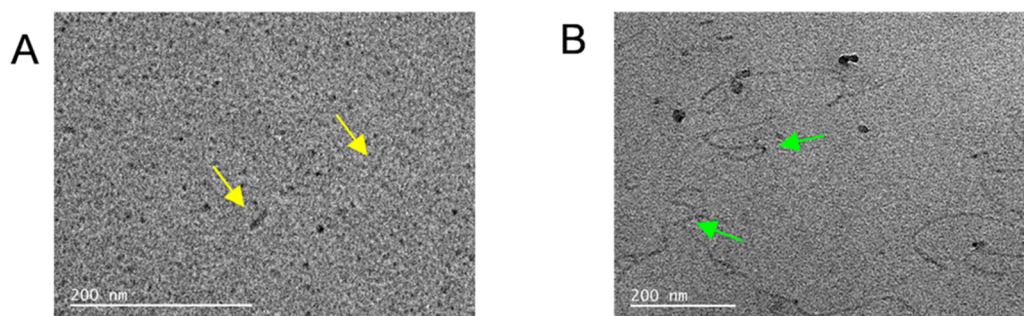


Figure 3. CryoTEM images of 0.25% SLE1S micelles (A) in 3.10% NaCl, showing spherical or rod-shaped micelles (yellow arrows) and (B) in 6.13% NaCl showing wormy micelle chains with occasional branching (green arrows).

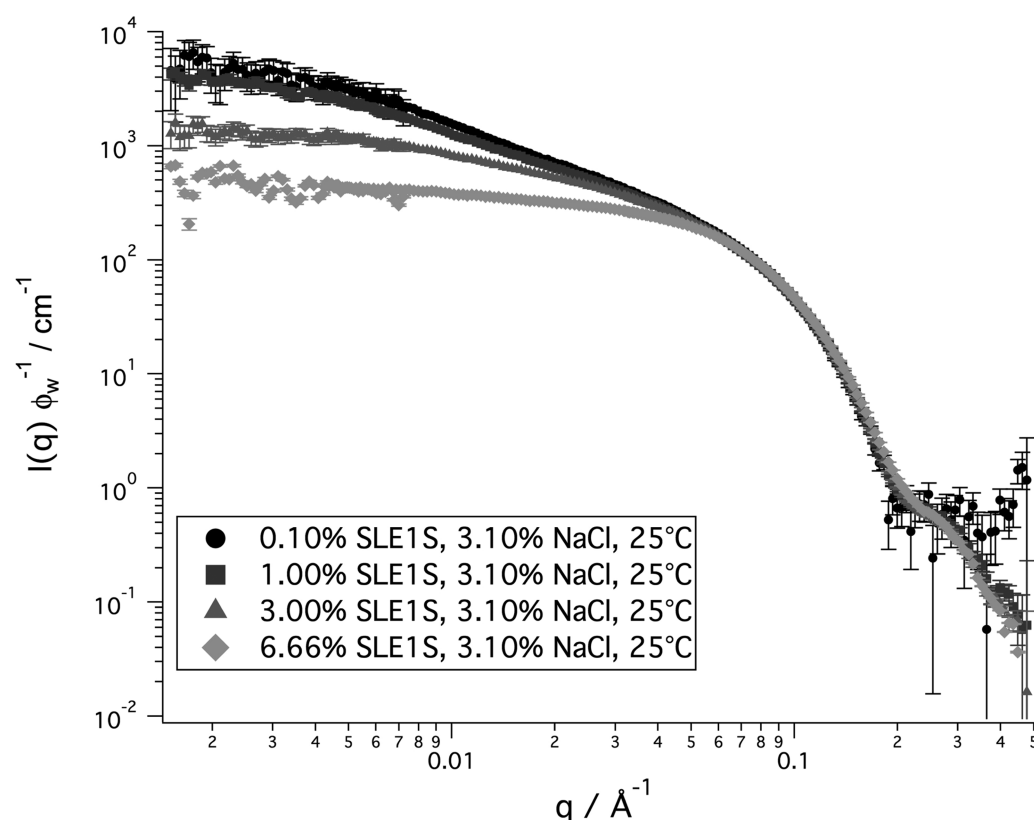


Figure 4. Scattering intensities $I(q)$ vs q for a concentration series of SLE1S in D_2O .

initially toward lower ϕ before falling off monotonically to $\phi \approx 0.005$. For measurements performed at $\phi = 0.0025$ to 0.01 , the variation of η_{sp} is approximately linear in the double-logarithmic plot. The corresponding slope of ~ 2.7 , less than the value predicted for linear micelles, is a consequence of the presence of branching. The flattening of the curve at concentrations between $\phi = 0.01$ and 0.067 may be due to the formation of a saturated network of multiconnected micelles. All in all, the specific viscosity curve is complicated by several factors including the presence of branching and the high ionic strength of the solution. At slightly higher salt concentrations, these micellar solutions phase separate. Generally, it has been considered that the overlap concentration occurs when $\eta_{sp} \approx 1$ or when the solution viscosity is about twice the viscosity of the solvent for linear synthetic polymers.²⁶ These micellar solutions differ from linear synthetic polymers because the chains grow with increasing solvent concentration and, in the 6.13% NaCl case, the chains are branched. It is therefore

difficult to estimate the overlap concentration or the entanglement concentration from the 6.13% NaCl data in Figure 2.

CryoTEM data collected on 0.25% SLE1S at 3.10 and 6.13% NaCl/ D_2O ($\phi = 0.0025$) are depicted in Figure 3. The 6.13% sample displays unentangled, nonoverlapping wormlike chains for a concentration about in the center of the 6.13% NaCl curve in Figure 2, further supporting the concept that a simple interpretation concerning chain entanglement is not possible from this high NaCl concentration curve. Both of the micrographs in Figure 3 are for surfactant concentrations (approximately 8.15 and 8.31 mM) that are well above the critical micelle concentration for SLE1S in NaCl solutions in deionized H_2O of approximately 4 mM.²⁷ At these low concentrations, wormy micelles are evident at 6.13% NaCl but only rodlike or spherical micelles are observed with 3.10% NaCl. This qualitatively agrees well with findings from SANS (see below) where just small WLMs with a few subunits are

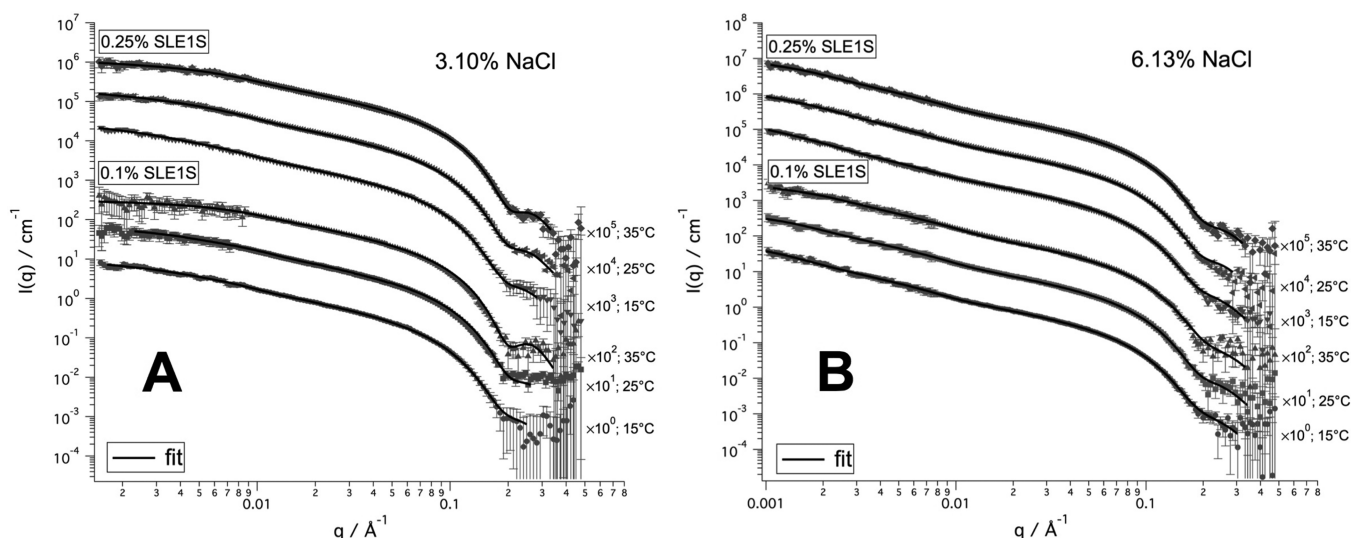


Figure 5. Scattering intensity $I(q)$ vs q for 0.1 and 0.25% SLE1S in the presence of (A) 3.10 and (B) 6.13% NaCl at different temperatures. The black lines denote fits applied via the hybrid scattering function.²⁰

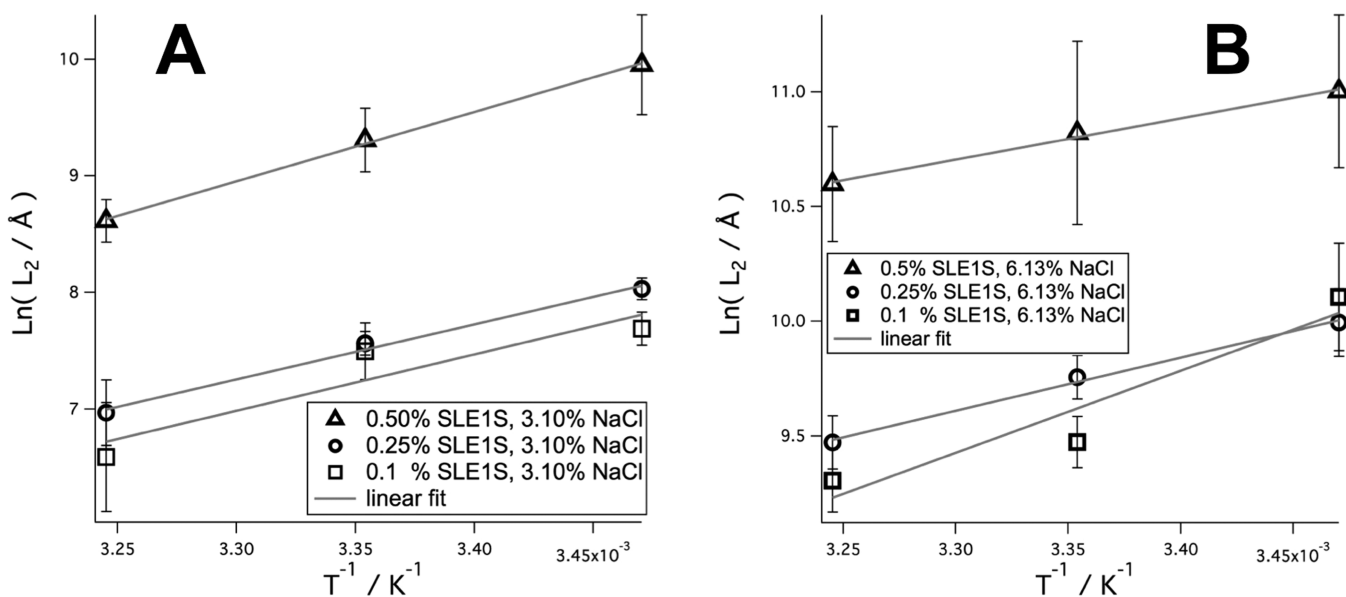


Figure 6. Plots according to relation 1 for SLE1S in the presence of (A) 3.10% NaCl and (B) 6.13% NaCl.

found at 3.01% NaCl but much larger ones are found at 6.13%. However, microscopy images allow the sampling of only a small fraction of the total population of micelle chains. Moreover, the sample volume is spread into a meniscus with a thickness in the micrometer range, which is of the same order of magnitude as the contour length for the WLMs. Significant shear and surface tension distortions might be expected in the TEM samples. SANS can be used to quantify micelle structure in bulk.

Neutron Scattering. Figure 4 depicts the concentration-normalized scattering intensities for a concentration series of SLE1S from 0.1 to 6.66 wt %. Although the normalized $I(q)$ agree well for concentrations of between 0.1 and 0.5% of surfactant, the normalized intensities at low q decrease and flatten out for concentrations above 0.5 wt %. This behavior is attributed to the occurrence of structural screening between 0.5 and 1 wt % of surfactant under the given conditions. This type of screening is similar to the overlap of WLMs in TEMs of higher-concentration samples, which reduces the ability to

identify individual chains. The designated structural screening stems from polymer science where the above behavior is observed at concentrations larger than the overlap concentration.²⁸ This effect hinders the assessment of large-scale structural features. Accordingly, just the data from samples under approximately dilute conditions (0.1 and 0.25 wt % of surfactant) were analyzed using the hybrid function.²⁰ The scattering intensities $I(q)$ for 0.5 wt % SLE1S exhibited weak screening, as indicated by the results from rheology (see above). This different scattering scenario can be taken into account via the random phase approximation (RPA).²⁸ If the plateau level at low q (Figure 4) can be reasonably approximated, then the scattering intensity $I(q)$ at the semidilute concentration ϕ_v can be fitted according to the formula

$$I(q) = \frac{1}{\frac{1}{I'(q)} + \nu} \quad (8)$$

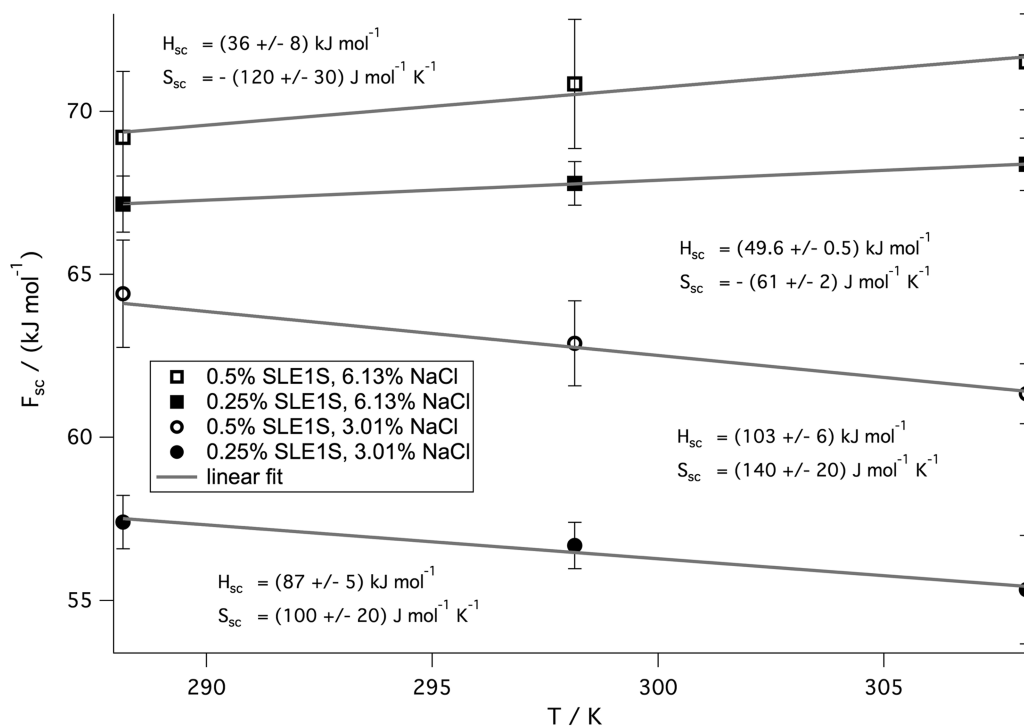


Figure 7. Free energies of scission F_{sc} according to eq 7 for 0.25 and 0.5% SLE1S at 3.10% NaCl as well as 6.13 wt % NaCl in D₂O. (0.10% SLE1S is not included because of poor statistics as mentioned with reference to Figure 6.)

where $I(q)$ is the scattering intensity for a hypothetical ideally dilute case as described in ref 20 and ν is the screening constant. The latter value is determined by approximating the plateau value at low q with a horizontal tangent. The screening constant ν is then given by the respective reciprocal with units of [cm]. This approach is limited to conditions where $I(q)$ in eq 8 is sufficiently large so that $I(q \rightarrow 0) \approx \nu^{-1}$. For 0.5% SLE1S in the presence of 3.1 and 6.13% NaCl fits according to eq 8 were performed (Figure 1 in the Supporting Information). At 6.13% NaCl, the plateau level was close to or below the lower q limit of the SANS measurements so that corresponding values of ν could just be approximated. We leave a detailed discussion of the properties and implications of ν for a future publication and just denote the results in Tables 3 and 4 of the Supporting Information.

Scattering intensities $I(q)$ vs q and the respective fits are shown in Figure 5 for 0.1 and 0.25 wt % SLE1S in the presence of different salt concentrations (3.10 and 6.13% NaCl) as well as at different temperatures (15, 25, and 35 °C). Tables 1–4 in the Supporting Information summarize the fitting results for 0.1, 0.25, and 0.5 wt % SLE1S at 15, 25, and 35 °C in the presence of the different salt concentrations (3.10 and 6.13 wt %). The changes with temperature as well as with surfactant and salt concentration are as expected. The contour and subunit lengths decrease monotonically with increasing temperature, whereas the contour length and subunit length decrease monotonically for both the salt and surfactant concentrations. The length L_1 varies between about 750 and 500 Å. The change in the salt concentration has a drastic impact on the contour length. At 3.10% salt and 0.25% surfactant, the number of subunits changes from 5 to 2 between 15 and 35 °C and to 30 and 20 at 6.13% NaCl. At 3.1% NaCl, increasing the surfactant concentration from 0.1 to 0.5 wt % induces an increase in L_1 from about 500 to 670 Å at 25 °C, whereas the number of subunits increases by roughly a factor of

4. Figure 6 depicts plots of the natural logarithm of the contour length L_2 vs the reciprocal temperature. The error bars are large for 0.1 wt % SLE1S. On the one hand, the signal-to-noise ratio is low at low surfactant concentration, and on the other hand, the salt to surfactant ratio is comparatively large, inducing the formation of large assemblies. That in turn shifts the Guinier region of $I(q)$ to lower q , below the experimentally accessible region, so that the inaccuracies for the large-scale structural parameters are accordingly very large. This, in combination with having just three data points, allows an estimation of only the order of magnitude for the values of H_{sc} . For 0.25 and 0.5 wt % of surfactant, the quality of the data is better. Accordingly, better statistics are obtained, and the data points in the semilog plot of L_2 vs T^{-1} exhibit a linear dependence to a better approximation (Figure 6). For temperatures above 15 °C, the branch content n_{br} can be calculated from the fitting values; however, error bars are too large for an unambiguous evaluation.

For 0.1 wt % SLE1S, the values for H_{sc} are (80 ± 30) kJ mol⁻¹ (3.10% NaCl) and (60 ± 20) kJ mol⁻¹ (6.13% NaCl). The error bars are large, and the two values found for the different salt concentrations do not differ significantly from each other. All in all, the values are in a range expected for high salt conditions.¹⁶ For 0.25 wt % SLE1S, H_{sc} equals (78 ± 7) kJ mol⁻¹ (3.10 wt % NaCl) and (38 ± 3) kJ mol⁻¹ (6.13 wt % NaCl). The enthalpy found at 3.10% NaCl is nearly twice the value of the respective one at 6.13% NaCl. At 0.5 wt %, SLE1S enthalpies H_{sc} of (98 ± 3) kJ mol⁻¹ (3.1% NaCl) and (30 ± 2) kJ mol⁻¹ (6.13% NaCl) were obtained. Within error bars, the enthalpy is between 10 and 20 kJ mol⁻¹ larger for 0.5% SLE1S as compared to that of the 0.25% surfactant. The difference reflects the different lengths found at higher surfactant concentration because an increase in contour length is driven by an increase in scission and end-cap energy.

As previously pointed out in the literature,^{16,17} solving for E_{sc} according to the scaling equation (eq 1) leads to counter-intuitive results. First, the scission energy is larger at the lower salt concentration. This would imply a larger contour length at 3.10% NaCl, which does not agree with the fitting results nor with the known impact of NaCl.² Second, the theoretical ratio of L_2 at 6.13 and 3.10% NaCl is nearly 1/3000 for 0.25% SLE1S, whereas from the direct structural fitting results for L_2 a ratio of ~ 9 can be calculated for 25 °C. Our finding agrees with the statement of Couillet et al. that large scission energies are found for low-ionic-strength systems and vice versa.¹⁷ To determine whether these inconsistencies can be explained by the lack of an entropic contribution in relations 1 and 2, plots according to eq 7 including the fits of the data points via linear regression are depicted in Figure 7.

The data points are consistent with a linear relationship. As expected, the free energies F_{sc} now have a larger value at higher salt concentration. Moreover, the correct ratios for L_2 under the two different conditions are now obtained. The differences between the enthalpy values obtained according to relation 1, assuming that $H_{sc} = E_{sc}$, and according to eq 5 are 10 and 30% for 3.10 and 6.13% NaCl at 0.25% SLE1S, respectively. For 0.5 wt % SLE1S and 3.10% NaCl, which are nearly identical (98 and 102 kJ mol⁻¹, respectively), in the presence of 6.13% NaCl the two values match within error bars. A semilogarithmic plot of $\ln L_2$ vs T^{-1} according to relation 1 is thus capable of determining H_{sc} in satisfactory approximation in the present case. Note that for 0.25 and 0.5 wt % SLE1S in the presence of 3.10% NaCl, the entropies are nearly identical within the given accuracy. The main difference with respect to the free energy F_{sc} under the observed conditions stems from the enthalpic contribution.

Complementing E_{sc} with an entropic part yields consistent results for L_2 under different conditions, but the question is whether the values obtained for S_{sc} have physical meaning, in particular the observed change in the sign of S_{sc} . The main difference between these two samples is the presence of chain branching under the high salt conditions. As mentioned earlier, chain scission in branched WLMs might be expected to be dominated by the stripping of branches from the chains, which leads to the formation of a single end-cap rather than two end-caps. In this scenario, half the enthalpy of scission might be expected for branched WLMs. Moreover, the removal of a branch eliminates many identifiable chain states associated with the free translation of the branch point along the wormlike micelle chain. This could result in a negative change in entropy on chain scission (branch stripping). However, these issues cannot be resolved here. Literature values for direct comparison of the entropy of chain scission are not available for any surfactant system to the best of our knowledge. Moreover, the entropic contributions from counterions and hydration in an aqueous environment are far from trivial.

The Bjerrum length is longer than the Debye screening lengths, which are about 4 and 3 Å for 3.1 and 6.13% NaCl, respectively, so that established models such as the Manning and Poisson–Boltzmann theories cannot be applied.²⁹ Works dealing with ion condensation and polyelectrolytes under high salt conditions are scarce, and a widely agreed upon model has not yet been established.^{30–33} It is possible to make a qualitative comparison only with the enthalpies H_{sc} published for other surfactant systems.^{12–19} These indirect determinations employing rheological data were performed at higher surfactant concentrations so that the issue of the concentration

dependence of H_{sc} or F_{sc} needs to be considered. Some hint of the behavior is given for the samples in Figure 7, which indicates an increase in the enthalpy change on scission with surfactant concentration, consistent with an increase in contour length. For a gemini surfactant system, Kern et al. report a nearly linear decline of H_{sc} as a function of surfactant concentration in a volume fraction range of between 0.05 and 0.1, a concentration range over a decade larger than that employed in the present work.¹¹ For the SLE1S system in this study, the opposite trend can be observed between 0.1 and 6.66 wt %. The rheological data in Figure 2 indicate an increase in contour length L_2 with increasing surfactant as well as salt concentration, in accordance with the SANS results. This finding would agree with an increasing enthalpy or free energy of scission with increasing surfactant concentration in the given concentration range. This finding might be due to the large salt concentrations employed in the present work, where the Bjerrum length is below the average distance between two headgroups (see paragraph above). A systematic study of F_{sc} as a function of surfactant as well as salt concentration could provide estimations of these energies for higher, rheologically more relevant concentrations via extrapolation. At this point, it can just be stated that the trends found via SANS are consistent with rheological findings in the literature.

CONCLUSIONS

It was found that WLM contour lengths display Arrhenius behavior, consistent with eq 1, and result in scission free energies similar to those found for other systems in the literature by rheological measurements. However, these energy values predict unreasonable contour lengths for the WLMs. Equation 1 is derived from an analytic function for the number of surfactant molecules in a WLM. This function can be determined exactly using SANS (eq 7). Equation 7 was used to determine the entropy and the enthalpy change on scission for WLMs. This approach results in reasonable values for enthalpy that can predict the observed WLM contour lengths. It is further found that significant differences in the change in enthalpy and entropy in chain scission exist between branched and linear WLMs that may reflect on underlying mechanistic differences.

This article has demonstrated that SANS is a direct and viable approach to obtaining both the enthalpy and the entropy change on chain scission for WLMs. The main disadvantages of SANS are the high cost and large amount of time required for the measurement and the limitation of the SANS measurement to concentrations near or below the chain overlap and entanglement concentrations. Extrapolation of these results to higher concentrations of rheological and commercial significance may be possible.

ASSOCIATED CONTENT

Supporting Information

The Supporting Information is available free of charge on the ACS Publications website at DOI: 10.1021/acs.langmuir.6b01169.

Fitting parameters and calculated values (PDF)

AUTHOR INFORMATION

Corresponding Authors

*E-mail: karsten.vogtt@uc.edu.

*E-mail: beaucag@uc.edu.

ORCID 

Karsten Vogtt: 0000-0003-3206-1070

Notes

The authors declare no competing financial interest.

■ ACKNOWLEDGMENTS

We thank Dr. Durgesh Rai from Oak Ridge National Laboratory for his support during the SANS measurements and with the data reduction. We also thank Bob Reeder (Procter & Gamble) for producing the cryoTEM images and interpretation. This research at ORNL's High Flux Isotope Reactor was sponsored by the Scientific User Facilities Division, Office of Basic Energy Sciences, U.S. Department of Energy.

■ REFERENCES

- (1) Bergström, L. M. Explaining the growth behavior of surfactant micelles. *J. Colloid Interface Sci.* **2015**, *440*, 109–118.
- (2) Dreiss, C. A. Wormlike micelles: where do we stand? Recent developments, linear rheology and scattering techniques. *Soft Matter* **2007**, *3* (8), 956–970.
- (3) Ezrahi, S.; Tuval, E.; Aserin, A. Properties, main applications and perspectives of worm micelles. *Adv. Colloid Interface Sci.* **2006**, *128–130*, 77–102.
- (4) Yang, J. Viscoelastic wormlike micelles and their applications. *Curr. Opin. Colloid Interface Sci.* **2002**, *7* (5–6), 276–281.
- (5) Carale, T. R.; Blankschtein, D. Theoretical and experimental determinations of the crossover from dilute to semidilute regimes of micellar solutions. *J. Phys. Chem.* **1992**, *96* (1), 459–467.
- (6) Rogers, S. A.; Calabrese, M. A.; Wagner, N. J. Rheology of branched wormlike micelles. *Curr. Opin. Colloid Interface Sci.* **2014**, *19* (6), 530–535.
- (7) Cates, M. E.; Candau, S. J. Statics and dynamics of worm-like surfactant micelles. *J. Phys.: Condens. Matter* **1990**, *2* (33), 6869–6892.
- (8) Candau, S. J.; Hirsch, E.; Zana, R.; Delsanti, M. Rheological properties of semidilute and concentrated aqueous solutions of cetyltrimethylammonium bromide in the presence of potassium bromide. *Langmuir* **1989**, *5* (5), 1225–1229.
- (9) Candau, S. J.; Merikhi, F.; Waton, G.; Lemarechal, P. Temperature-jump study of elongated micelles of cetyltrimethylammonium bromide. *J. Phys.* **1990**, *51* (10), 977–989.
- (10) Kern, F.; Zana, R.; Candau, S. J. Rheological properties of semidilute and concentrated aqueous solutions of cetyltrimethylammonium chloride in the presence of sodium salicylate and sodium chloride. *Langmuir* **1991**, *7* (7), 1344–1351.
- (11) Kern, F.; Lequeux, F.; Zana, R.; Candau, S. J. Dynamical properties of salt-free viscoelastic micellar solutions. *Langmuir* **1994**, *10* (6), 1714–1723.
- (12) Hassan, P. A.; Valaulikar, B. S.; Manohar, C.; Kern, F.; Bourdieu, L.; Candau, S. J. Vesicle to micelle transition: Rheological investigations. *Langmuir* **1996**, *12* (18), 4350–4357.
- (13) Soltero, J. F. A.; Puig, J. E.; Manero, O. Rheology of the cetyltrimethylammonium tosylate-water system. 2. Linear viscoelastic regime. *Langmuir* **1996**, *12* (11), 2654–2662.
- (14) Oda, R.; Narayanan, J.; Hassan, P. A.; Manohar, C.; Salkar, R. A.; Kern, F.; Candau, S. J. Effect of lipophilicity of the counterion on the viscoelasticity of micellar solutions of cationic surfactants. *Langmuir* **1998**, *14* (16), 4364–4372.
- (15) Raghavan, S. R.; Kaler, E. W. Highly viscoelastic wormlike micellar solutions formed by cationic surfactants with long unsaturated tails. *Langmuir* **2001**, *17* (2), 300–306.
- (16) Oelschlaeger, Cl.; Waton, G.; Candau, S. J. Rheological Behavior of Locally Cylindrical Micelles in Relation to Their Overall Morphology. *Langmuir* **2003**, *19* (25), 10495–10500.
- (17) Couillet, I.; Hughes, T.; Maitland, G.; Candau, F.; Candau, S. J. Growth and scission energy of wormlike micelles formed by a cationic surfactant with long unsaturated tails. *Langmuir* **2004**, *20* (22), 9541–9550.
- (18) Siriawatwechakul, W.; LaFleur, T.; Prud'homme, R. K.; Sullivan, P. Effects of organic solvents on the scission energy of rodlike micelles. *Langmuir* **2004**, *20* (21), 8970–8974.
- (19) Oelschlaeger, C.; Suwita, P.; Willenbacher, N. Effect of counterion binding efficiency on structure and dynamics of wormlike micelles. *Langmuir* **2010**, *26* (10), 7045–7053.
- (20) Vogtt, K.; Beaucage, G.; Weaver, M.; Jiang, H. Scattering Function for Branched Wormlike Chains. *Langmuir* **2015**, *31* (30), 8228–8234.
- (21) Kholodenko, A. L. Analytical calculation of the scattering function for polymers of arbitrary flexibility using the Dirac propagator. *Macromolecules* **1993**, *26*, 4179–4183.
- (22) Jerke, G.; Pedersen, J. S.; Egelhaaf, S. U.; Schurtenberger, P. Static structure factor of polymerlike micelles: Overall dimension, flexibility, and local properties of lecithin reverse micelles in deuterated iso-octane. *Phys. Rev. E: Stat. Phys., Plasmas, Fluids, Relat. Interdiscip. Top.* **1997**, *56* (5), 5772–5788.
- (23) Lequeux, F. Reptation of connected wormlike micelles. *Europhys. Lett.* **1992**, *19* (8), 675–681.
- (24) Cates, M.; Fielding, S. Theoretical Rheology of Giant Micelles. In *Giant Micelles*; Kaler, E. W., Zana, R., Eds.; CRC Press, 2007; pp 109–162.
- (25) Helgeson, M. E.; Hodgdon, T. K.; Kaler, E. W.; Wagner, N. J. A systematic study of equilibrium structure, thermodynamics and rheology of aqueous CTAB/NaNO₃ worm like micelles. *J. Colloid Interface Sci.* **2010**, *349*, 1–12.
- (26) Colby, R. H. Structure and linear viscoelasticity of flexible polymer solutions: comparison of polyelectrolyte and neutral polymer solutions. *Rheol. Acta* **2010**, *49*, 425–442.
- (27) Barry, B. W.; Wilson, R. C.M.C., counterion binding and thermodynamics of ethoxylated anionic and cationic surfactants. *Colloid Polym. Sci.* **1978**, *256*, 251–260.
- (28) Fujita, H. *Polymer Solutions*; Elsevier Science Publishers B.V.:Amsterdam, The Netherlands, 1990; pp 195–197.
- (29) Manning, G. S. The molecular theory of polyelectrolyte solutions with applications to the electrostatic properties of polynucleotides. *Q. Rev. Biophys.* **1978**, *11* (2), 179–246.
- (30) Fenley, M. O.; Manning, G. S.; Olson, W. K. Approach to the limit of counterion condensation. *Biopolymers* **1990**, *30* (13–14), 1191–1203.
- (31) Deserno, M.; Holm, C.; May, S. Fraction of condensed counterions around a charged rod: Comparison of Poisson-Boltzmann theory and computer simulations. *Macromolecules* **2000**, *33* (1), 199–206.
- (32) Ise, N.; Sogami, I. *Structure Formation in Solution: Ionic Polymers and Colloidal Particles*; Springer Science & Business Media: New York, 2005; pp 67–69.
- (33) Lamm, G.; Pack, G. R. Counterion condensation and shape within Poisson-Boltzmann theory. *Biopolymers* **2010**, *93* (7), 619–639.